Z. Phys. C – Particles and Fields 53, 277–286 (1992)

Zeitschrift für Physik C Particles and Fields

Numerical analysis of tunneling paths in constant field SU(2) lattice gauge theory

J. Bartels, O. Brüning, B. Raabe

II. Institut für Theoretische Physik der Universität Hamburg, Luruper Chaussee 149, W-2000 Hamburg 50, Federal Republic of Germany

Received 10 April 1991

Abstract. We present results of a computer analysis of euclidean solutions of the SU(2) lattice gauge theory Hamiltonian for constant fields. The accumulation of tunneling solutions in a certain region of phase space is investigated because it is expected to give a strong contribution to the path integral. Our analysis shows, that an infinite set of classical trajectories with finite action exists, and describes how they cluster.

1 Introduction

In the context of attempts to gain an analytic understanding of the quantum theory of nonabelian gauge fields, the SU(2) Yang-Mills Hamiltonian for spatially constant fields has attracted much interest. In particular the simplified form [1]

$$H=\tfrac{1}{2}(p_1^2+p_2^2+x_1^2 x_2^2) \tag{1}$$

has been investigated by many authors [2–5]. It has been shown that the classical Hamiltonian is nonintegrable [2], whereas the quantum Hamiltonian has a discrete energy spectrum [3, 7], which is reproduced by semiclassical methods surprisingly well [4].

One line of arguments which has motivated interest in this model is the small-volume approximation of Lüscher and Münster [6, 7] and Koller and van Baal [8, 9]. Starting point is the observation that for small volumes the effective coupling constant is small and hence allows the use of perturbation theory. In a systematic expansion in powers of $g^{2/3}$, all fields with nonzero momenta are integrated out, and one arrives at an effective Hamiltonian whose leading term is again the Hamiltonian of constant fields from which (1) is obtained by using gauge and rotational symmetry and setting one field component to zero. At very small volumes, the energy spectrum is governed solely by the (narrow) potential valley around the zero field point. At somewhat larger volumes, tunneling effects set in: the nontrivial structure of the classical vacuum (torons), in particular the discrete $\mathbf{Z}_2^3$ symmetry, leads to a tunneling from one part of the vacuum to others, and the adiabatic approximation allows a quantitative description of the splitting of the energy levels which is in good agreement with numerical calculations [9, 10]. Very unfortunately, however, comparison with Monte Carlo studies of lattice gauge theories [11] show that at a rather well-defined size of the system this description starts to fail, thus indicating that the tunneling contributions considered so far are no longer relevant. Apart from the conclusion that, most likely, the whole approach of using a low-dimensional effective Hamiltonian no longer works, one might also suspect that very different tunneling phenomena will become important which, in the small-volume limit, may already exist but are still subdominant.

Another motivation for studying the Hamiltonian (1) comes from an attempt [12] to investigate the small-coupling limit of lattice gauge theories using the semiclassical approximation. The way in which the bare lattice coupling constant g_0, which becomes small in the continuum limit, enters the lattice Hamiltonian is analogous to that of Planck's constant in the Schrödinger equation; this suggests to use the semiclassical approximation with g_0 as the small parameter. Moreover, the renormalization group equation predicts a g_0^2-dependence for physical quantities, which hints at tunneling phenomena.

Both these lines of arguments suggest that, if we want to study Yang-Mills quantum mechanics more thoroughly, we also need to analyse the solutions to the equations of motion in the classically forbidden region. The natural starting point for investigating tunneling phenomena is the (somewhat simplified) version of the lattice Hamiltonian for constant fields [12]

$$H=\frac{g_0^2}{2}(p_1^2+p_2^2)+\frac{2}{g_0^2}\cos^2\theta_1\cos^2\theta_2, \tag{2}$$

where the variables θ_i range from $-\pi/2$ to $\pi/2$. The continuum Hamiltonian (1) is recovered from (2) in the approximation of small fields where $|\theta_i|\simeq\pi/2$ after setting g_0^2 equal to 2 and rescaling by a factor 1/2. The classically

forbidden region of this Hamiltonian has first been analyzed in [12] in the region of small fields, and one of the striking features observed was the clustering of instanton-like solutions along the diagonal line $\theta_1=\theta_2$, which connects the point of zero field strength $\theta_1=\theta_2=-\pi/2$ with the (gauge equivalent) south pole at $\theta_1=\theta_2=+\pi/2$ (see Fig. 1). The contribution of such a set of classical solutions to quantum mechanical quantities (e.g. the partition function Z) is completely unknown. On the other hand, one can show [13] that such a clustering is not an artifact of the constant field lattice Hamiltonian but extends into the space of non-constant fields. Therefore a careful analysis of such a situation, e.g. in the spirit of the work of Polyakov [14] and Coleman [15], seems highly desirable.

Naively one expects that the existence of several nearby extrema of the action integral makes the usual evaluation of gaussian fluctuations around stationary points impossible. Even if each solution represents a genuine extremum of the action, eigenvalues of the second variation are expected to be small, hence the fluctuations are large. Consequently, the condensation of such an infinite number of solutions is expected to give a large contribution to the partition function: one may even speculate that if the solutions are sufficiently dense, their sum may compete with the factor $\exp(-S/g_0^2)$. Whether two single extrema can be 'resolved' or not depends both on the 'distance' between the two extrema and the smallness of the 'resolution' parameter g_0. This leads to a new g_0^2-dependence of the sum of the classical solutions. Before this difficult task of summing over all solutions and calculating their contribution to the semiclassical approximation of any quantum mechanical quantity can be attacked, a careful study of the classical solutions and their condensation is inevitable.

In this paper we report on the results of a computer analysis of the trajectories in the classically forbidden region and discuss the main implications of our study. This analysis should be seen as the necessary prerequisit for the summation over the infinite number of classical paths. Let us briefly outline the strategy for the numerical study. Following Polyakov [14] and Coleman [15], we are interested in classical solutions which need an infinite amount of time to travel from one maximum of the inverted potential to another, thereby giving a finite action integral. In the Hamiltonian (2) these are solutions with energy zero. They represent, however, just the separatrix between rotation and liberation and, hence, are the most difficult to study. We therefore start our analysis at the bottom of the potential at energy $E=-1/2$, where the system is nearly integrable. We then vary the energy and follow the flow of solutions up to $E=0$. In the beginning we can use canonical perturbation theory to analyse the solutions, but as the energy increases more and more KAM tori are destroyed and an analytic treatment becomes impossible. At $E=0$, the system is stochastic in the vicinity of the diagonal line, which we are interested in. However, inside this chaotic region, an infinite number of solutions exist which condensate on the diagonal, and there is a remarkably regular, self-similar pattern in the way in which they accumulate.

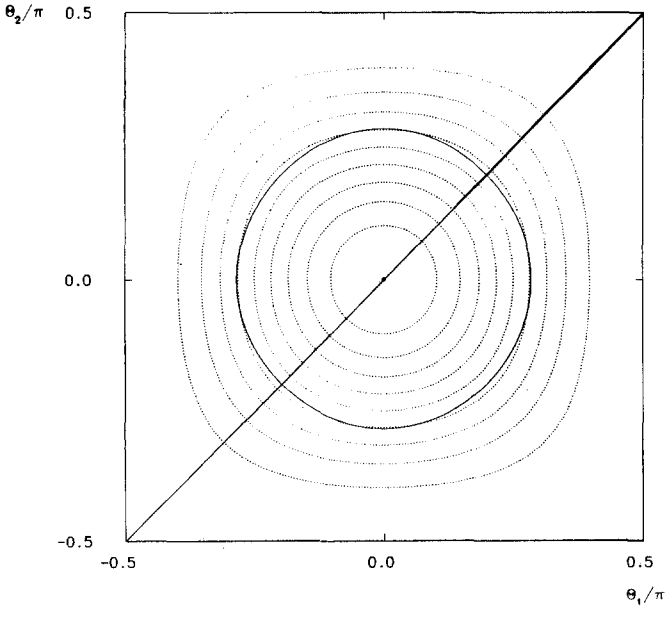

Fig. 1. Equipotential lines in the $\theta_1-\theta_2$-plane (dotted lines). The full curves represent a diagonal and the circular solution for $E=0$

2 Analysis of the trajectories in the classically forbidden region

For our study of the Hamiltonian (2) in the classically forbidden region we choose $g_0^2=2$, reverse the sign of the potential to avoid the use of imaginary time and rescale H by a factor of 1/2 so that it reads

$$H=\tfrac{1}{2}(p_1^2+p_2^2-\cos^2\theta_1\cos^2\theta_2). \tag{3}$$

We first of all note, that for small energies ($E\simeq E_{\min}=-1/2$) θ_1 and θ_2 only move in the center of the potential, where it may be approximated by its Taylor expansion. Consequently θ_1 and θ_2 behave like two weakly coupled harmonic oscillators with a coupling strength of order $(\Delta E)^2$, where $\Delta E=E-E_{\min}$. For $\Delta E\ll 1$ the system is therefore close to an integrable one and may be treated via perturbation theory [16, 17] with ΔE as a small parameter. In combination with numerical calculations this allows us to understand the behaviour of the solutions of the equations of motion for $E\to 0$.

By a sequence of canonical transformations it is possible to reduce the Hamiltonian to the form

$$H=J_2-\tfrac{1}{4}J_2^2-\tfrac{1}{2}+\tfrac{1}{4}(J_1^2-J_1J_2)\cos(2\psi_1)+\mathcal{O}((\Delta E)^3)$$

and thereby remove all dependence on the angle variable ψ_2 to $\mathcal{O}((\Delta E)^2)$. Here $J_1=I_1+\mathcal{O}((\Delta E)^2)$, $J_2=I_1+I_2+\mathcal{O}((\Delta E)^2)$, $\psi_1=\varphi_1-\varphi_2+\mathcal{O}((\Delta E)^2)$ and $\psi_2=\varphi_2+\mathcal{O}((\Delta E)^2)$, where I_i and φ_i are the action and angle variables of the unperturbed harmonic oscillators, respectively.

Because H is intrinsically degenerate, i.e. the unperturbed Hamiltonian $H_0=J_2-\frac{1}{4}J_2^2-\frac{1}{2}$ does not depend on the action variable J_1 (cp. [16, Sects. 2.4 and 3.2.a]) one cannot get rid of the ψ_1-dependent term. The resulting equations of motion for J_i and ψ_i may then be discussed

and translated back into approximate analytic expressions for p_i and θ_i. These can be used to compute the points where the phase space trajectories pierce a surface of intersection (SI) [16, 18] for which we choose $\theta_2 = 0$ and make no restriction on the sign of p_2. Comparison of this perturbatively constructed SI with the numerically computed one shows that for small ΔE virtually all invariant tori are preserved and Fig. 2 illustrates that even for ΔE as large as 1/4 they agree rather well.

To relate points and curves in the SI to certain solutions of the equations of motion, we now describe three

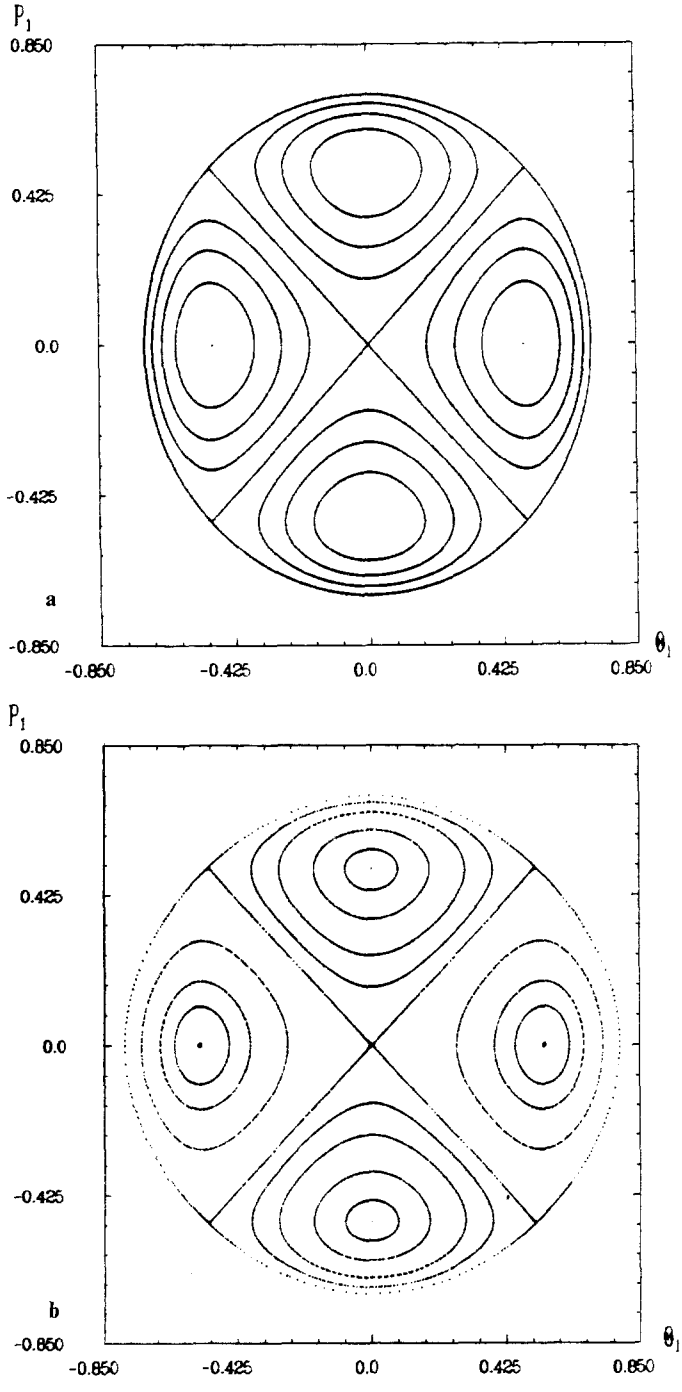

Fig. 2a, b. The surface of intersection for $E = -1/4$ **a** the perturbatively constructed SI. **b** the numerically computed SI

different types of trajectories distinguished by the symmetry of the potential (see Fig. 1). Those with $|\theta_1| = |\theta_2|$, the 'diagonal' solutions, correspond to the two elliptic fixpoints on the line $\theta_1 = 0$ in the SI. As can be read off from the analytic solution in terms of a Jacobian elliptic function (see [19, chs. 16 and 17])

$$\pm\theta_i(t) = \arctan\left\{\left(\frac{ab}{\sqrt{a^2+b^2}}\right)\mathrm{sd}\left(\frac{\sqrt{2}t}{\sqrt{a^2+b^2}}\middle|\frac{b^2}{a^2+b^2}\right)\right\}, \tag{4}$$

where

$$a^2 = \frac{1}{\sqrt{-2E}} + 1 \quad \text{and} \quad b^2 = \frac{1}{\sqrt{-2E}} - 1,$$

their frequency is 1 in the limit $E \to E_{\min}$ and vanishes as $E \to 0$, where (4) assumes the form

$$\pm\theta_i(t) = \arctan\left(\frac{\sqrt{2}t}{2}\right).$$

Neighbouring solutions oscillate orthogonal to them and either begin and end on the potential boundary (instantons) or get close to it for $E \to 0$.

A second stable solution which is approximately a circle in the $\theta_1 - \theta_2$-plane may be constructed with the help of a Fourier expansion. Neither it nor its neighbours ever reach the potential boundary and they therefore do not qualify as tunneling paths. The two elliptic fixpoints on the line $p_1 = 0$ correspond to this circular solution.

The unstable solutions with $\theta_1 = 0$ and $\theta_2 = 0$ get mapped onto the centre and the outer circle in the SI, respectively, which represent hyperbolic fixpoints.

Lowest order perturbation theory for this system always yields circular Poincaré sections. The numerical analysis, however, shows that with increasing $(\Delta)E$ they not only grow in size, but also their shape becomes more lenticular (see Fig. 3), which is to be expected because the boundary of the SI is given by the $(\theta_2 = 0)$-solution. For small energies it looks like the phase portrait of a harmonic oscillator with unit frequency, but for larger energies the nonlinearity of the pendulum becomes visible.

At the same time as one varies the energy from $E_{\min}$ to 0, more and more tori get destroyed. Tori with rational ratios of frequencies r/s given by small integers r and s break up first. For the integrable system any point on them is a fixed point. The Poincaré-Birkhoff theorem (see e.g. [16, Sect. 3.2]) states that upon destruction of a given torus an even number of fixed points remains unchanged, one half of them being elliptic, the other half hyperbolic. The tori around the circular solution prove to be more robust than those around the diagonals (Fig. 3). This is because the corresponding trajectories do not probe the potential boundary and thus less strongly feel the deviation of the potential from the integrable case.

In Fig. 3 one can see how with increasing energy the tori in the vicinity of the elliptic fixpoint distort and finally*

* Due to the limited numerical precision whenever we speak of the limit $E \to 0$ in the following, this will mean that the calculations have been performed at $E = -10^{-10}$

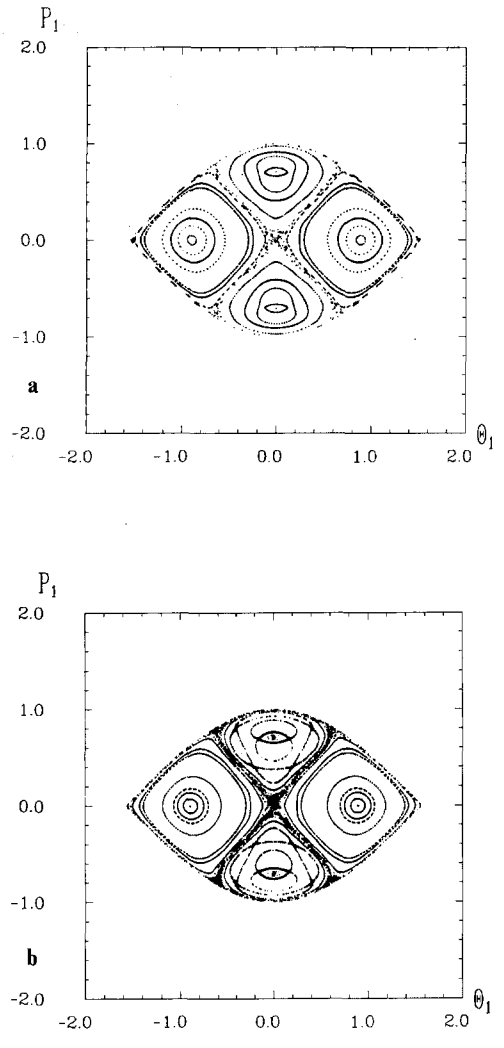

Fig. 3a, b. The surface of intersection for $E=-10^{-3}$; **b** The surface of intersection for $E=-10^{-10}$

for $E=-10^{-10}$ break up leaving a chain of two islands shown in (Fig. 4a). As the stable trajectory corresponding to them (see Fig. 4c) closes after one oscillation along the $(\theta_1=\theta_2)$-axis and two oscillations along the $(\theta_1=-\theta_2)$-axis, we will call it a (1:2)-resonance. It intersects the SI ($\theta_2=0$) with two different values of p_1, once with $p_1>0$ and once with $p_1<0$. Both intersection points lie on the $(\theta_1=0)$-axis, and coincide with the two elliptic fixpoints in Fig. 4a. Similarly the unstable trajectory in Fig. 4d intersects the SI once with $p_1<0$ and once with $p_1>0$; its intersection points coincide with one pair of the hyperbolic fixpoints in Fig. 4a. By reflecting the two trajectories on the $(\theta_1=\theta_2)$-axis, one creates a second pair of trajectories corresponding to the other four fixpoints in Fig. 4a. The same correspondence due to reflexion and time reversal symmetry applies to all other resonances to be mentioned later on.

So far, we have discussed the standard KAM scenario with its break-up of invariant tori due to increasing perturbation strength and applied it to the model at hand without specialising on certain trajectories. Our main interest, however, is in the hyperbolic fixpoints arising from resonances around the diagonal solutions. In the limit $E\to 0$ they correspond to trajectories beginning and ending on the potential boundary near the corner points and hence lead to tunneling paths expected to be relevant for the computation of observables in the underlying lattice gauge theory.

From the work of Polyakov [14] we know that for each tunneling path we have to take multiple transversals into account (cp. also Coleman's Erice lectures [15]). For a given time interval $[-T, T]$, we can find an infinite set of energies, for which such a solution begins on the potential boundary at $t=-T$, oscillates a given number of times back and forth through the potential valley, and ends on the potential boundary at $t=+T$. In the limit $T\to\infty$ all these solutions have the same energy $E=0$. Integrating over all instants at which n tunneling processes may occur yields a factor $T^n/n!$ which upon summation over n, to take all (anti-)instanton contributions into account, leads to an exponential energy split. As shown in [15] in the semiclassical limit the dominant contributions to the path integral come from configurations which are far apart. Thus, the extrema of the action are well separated and the fluctuations around the instantons are approximately gaussian. In our problem we not only have to take multiple transversals of a single trajectory into account, but moreover observe a spatial clustering of tunneling paths of almost the same action. The assumption on the well-separatedness of the extrema therefore becomes doubtful and we have to look for new ways to evaluate the path integral.

Because of the mechanical similarity [20] of the quadratic approximation of the potential near the corner-points ($|\theta_1|=\pi/2=|\theta_2|$), this clustering does not come unexpected [12]. We find an infinite set of trajectories, which correspond to $(1:n)$-resonances around the diagonal solutions with initial values closer and closer to the corner points. In contrast to the phenomenon considered by Polyakov and Coleman, we now have $E=0$ fixed and vary the order of the resonance n. The appearance of this infinite number of resonances leads to a nested set of self-similar SI's.

To illustrate this, we first look at the trajectories of the (1:2)-resonance (Fig. 4c and d). From the previous discussion we know that the elliptic fix-points of this resonance lie on, and the hyperbolic fixpoints symmetrically to the $(\theta_1=0)$-axis. The construction of the elliptic and hyperbolic fixpoints of the (1:3)-resonance now proceeds in complete analogy. The four unstable trajectories of the (1:3)-resonance (Fig. 5a plus the symmetry images; in the following we restrict our attention to the diagonal $\theta_1=\theta_2$. Trajectories oscillating around the other diagonal lead to the same points in the SI.) intersect the SI at $\theta_1=0$, the four stable trajectories intersect it symmetrically to the $(\theta_1=0)$-axis. Because the trajectories of the (1:3)-resonance start closer to the corner point $\theta_1=\theta_2=-\pi/2$ and lie closer to the diagonal than the trajectories of the (1:2)-resonance, the elliptic fixpoints of the (1:3)-resonance lie inside the region enclosed by the islands of the (1:2)-resonance. This picture is illustrated in Fig. 6. In Fig. 6a we see two islands of the (1:2)-resonance and in the region enclosed by them

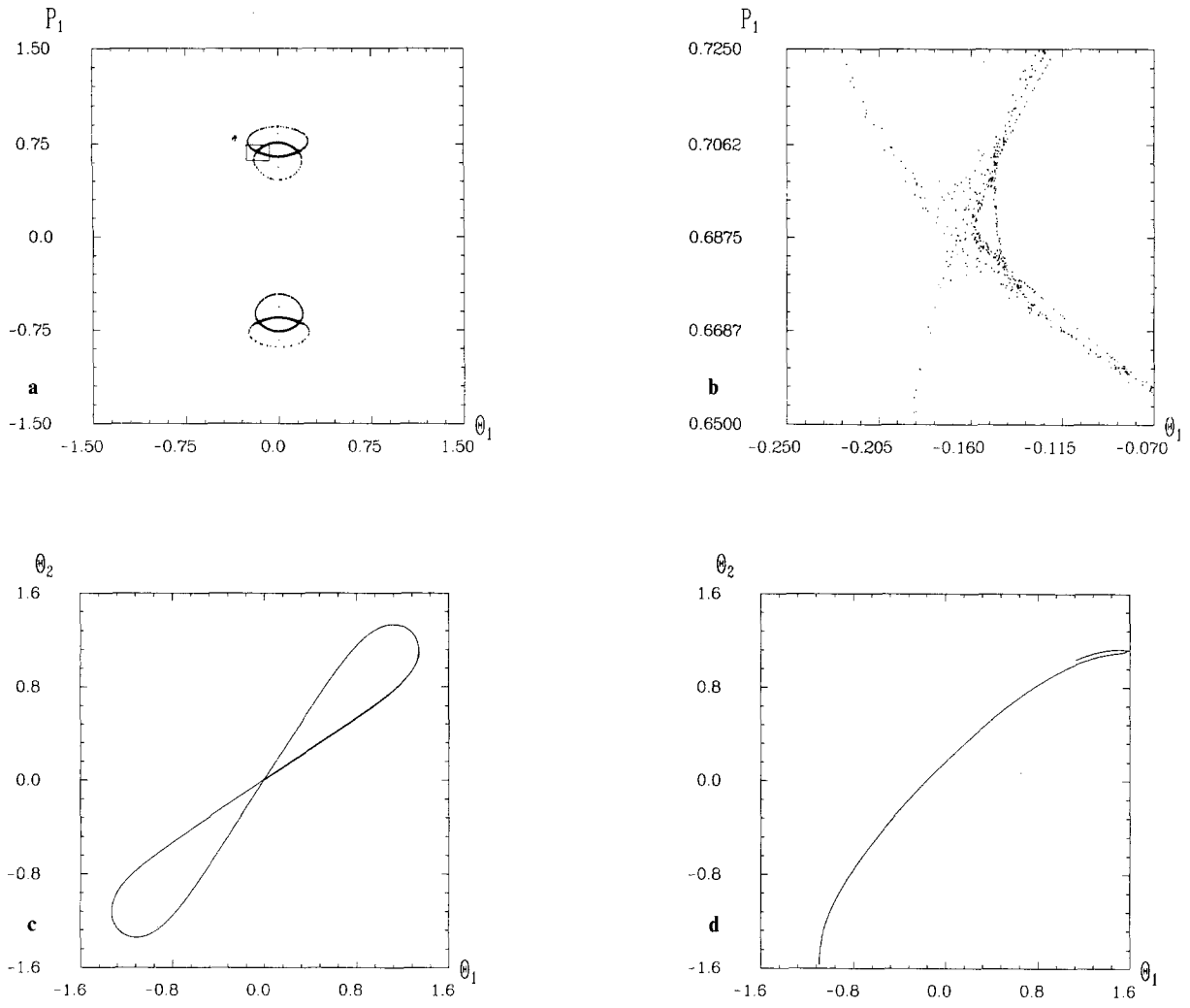

Fig. 4a–d. The (1:2)-resonance. **a** surface of intersection; **b** enlargement of a; **c** the elliptic trajectory; **d** the hyperbolic trajectory

the islands of the (1:3)-resonance. An enlargement* of this region (Fig. 6b) shows that the islands of the (1:3)-resonance look like those of the (1:2)-resonance rotated by $\pi/2$. An analogous discussion for the trajectories of the (1:4)-resonance (Fig. 5b) shows that the two islands of the (1:4)-resonance lie inside the region enclosed by the islands of the (1:3)-resonance, and that they are again rotated by $\pi/2$ (Fig. 6b).

With increasing values of n the trajectories start closer to the lower left corner of the potential and cluster along the diagonal solution for $n \to \infty$. Their strong oscillations orthogonal to the diagonals produce a rich structure of caustics [12]. As their actions are almost equal they should all be taken into account in any attempt to evaluate the path integral.

A similar discussion can be performed for *all* $(m:n)$-resonances. The numerical calculations confirm the clustering along the diagonal as $n \to \infty$ for any value of m. Again we observe that the starting points move towards the corner of the potential and see a nested set of self-similar SI's. In Fig. 7c and d, for example, we show the first two unstable trajectories for the $(2:n)$-resonances. They lead to the hyperbolic fixed points of Fig. 7a (Fig. 7b shows the inner chain of islands of Fig. 7a on a larger scale). The action of the $(m:n)$-resonance is roughly proportional to m.

But still another kind of clustering exists, which leads to an infinite set of intersecting trajectories in the neighbourhood of *any* trajectory that begins and ends on the potential boundary.

We illustrate this for the (2:3)-resonance. In Fig. 8a it is depicted in the middle of two other chains of islands, one surrounding it that corresponds to the (3:4)-resonance, and another one corresponding to the (3:5)-resonance that lies inside the region enclosed by the islands of the (2:3)-resonance. If we approach the (2:3)-resonance from these neighbouring chains of islands we find two more resonances shown in Fig. 8b: the (5:7)-resonance with its ten islands squeezed in between the (3:4)-resonance and the (2:3)-resonance and a barely visible (5:8)-resonance between the (2:3)- and the (3:5)-resonance. Repeating this procedure, one will always get new chains with ever higher

* Because the trajectories near the diagonal $\theta_1 = \theta_2$ are very sensitive to a variation of the initial conditions, the islands of the (1:3)-resonance in Fig. 6 are not as densely drawn as those of the (1:2)-resonance

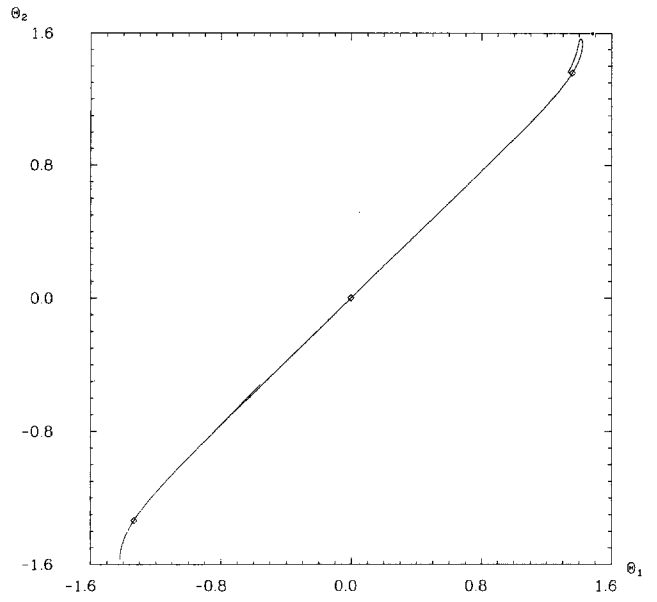

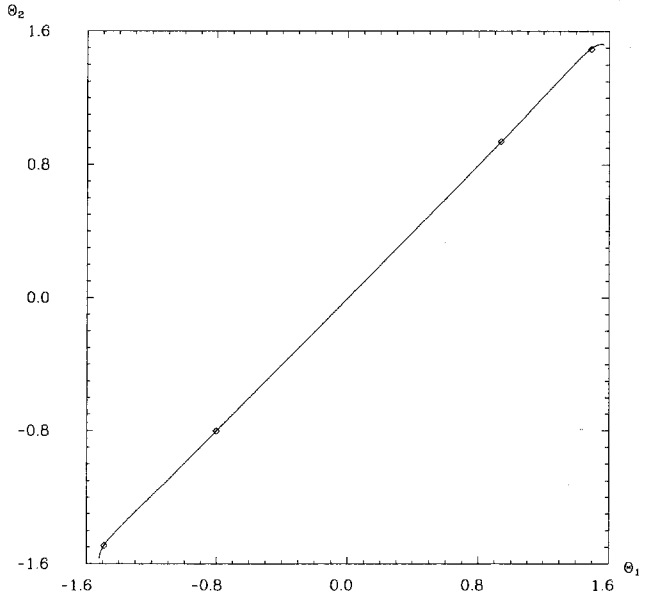

Fig. 5. Unstable trajectories (The dots on the trajectories mark the intersections with the diagonal.)

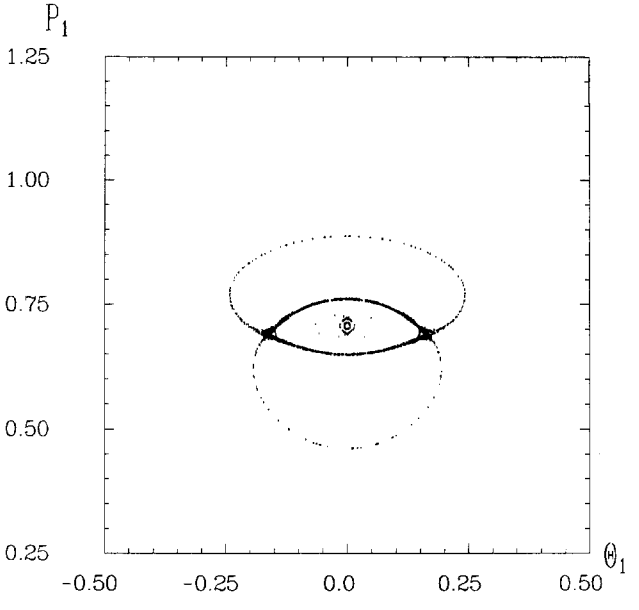

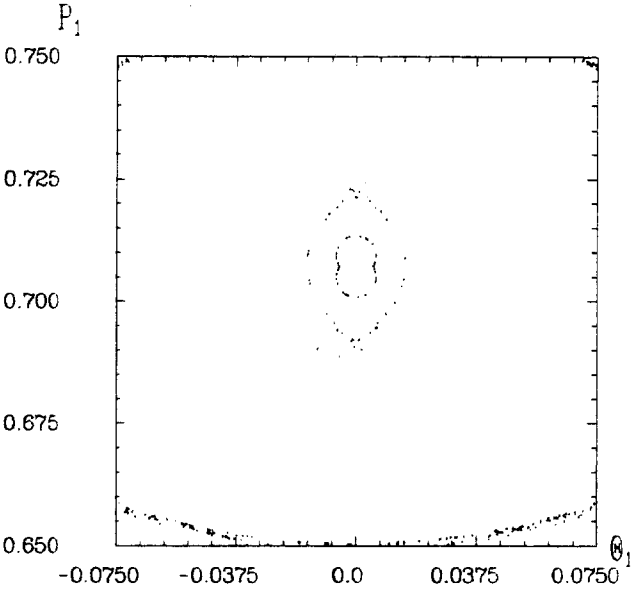

Fig. 6. The self-similarity of the SI for the $(1:n)$-resonances

numbers of islands. In Fig. 9 we show the corresponding trajectories for the two outer chains in Fig. 8. If we look at the trajectories' starting points on the $(\theta_2 = -\pi/2)$-axis (Fig. 9), we see that they lie the closer to the starting point of the (2:3)-trajectory (Fig. 7c), the closer the chain of islands lies to the islands of the (2:3)-resonance. The accumulation of islands around the islands of the (2:3)-resonance therefore leads to a clustering of starting points at the starting point of the unstable trajectory of the (2:3)-resonance. The trajectories intersect each other and have a diverging action for a vanishing distance of their starting point from the starting point of the (2:3)-trajectory.

Generally, an arbitrary $(m:n)$-resonance is surrounded by higher resonances. For any not too large rational number $q = m'/n'$ which cannot be reduced to lower terms we find an $(m':n')$-resonances with an initial point the closer to that of the $(m:n)$-resonance the better q approximates m/n. The SI's of all $(m:n)$-resonances with fixed m but varying n form a nested self-similar set, the SI's shrinking to the fixpoint of the diagonal as $n \to \infty$. Let us stress again, that for a proper evaluation of the path integral multiple transversals of single trajectories as well as the clustering of nearby but different trajectories should be taken into account. Whereas the former problem has been solved by Polyakov [14] the latter seems to be new and constitutes the phenomenon which is at the heart of this paper. Qualitatively we expect that the existence of nearby classical tunneling solutions leads to extrema of the

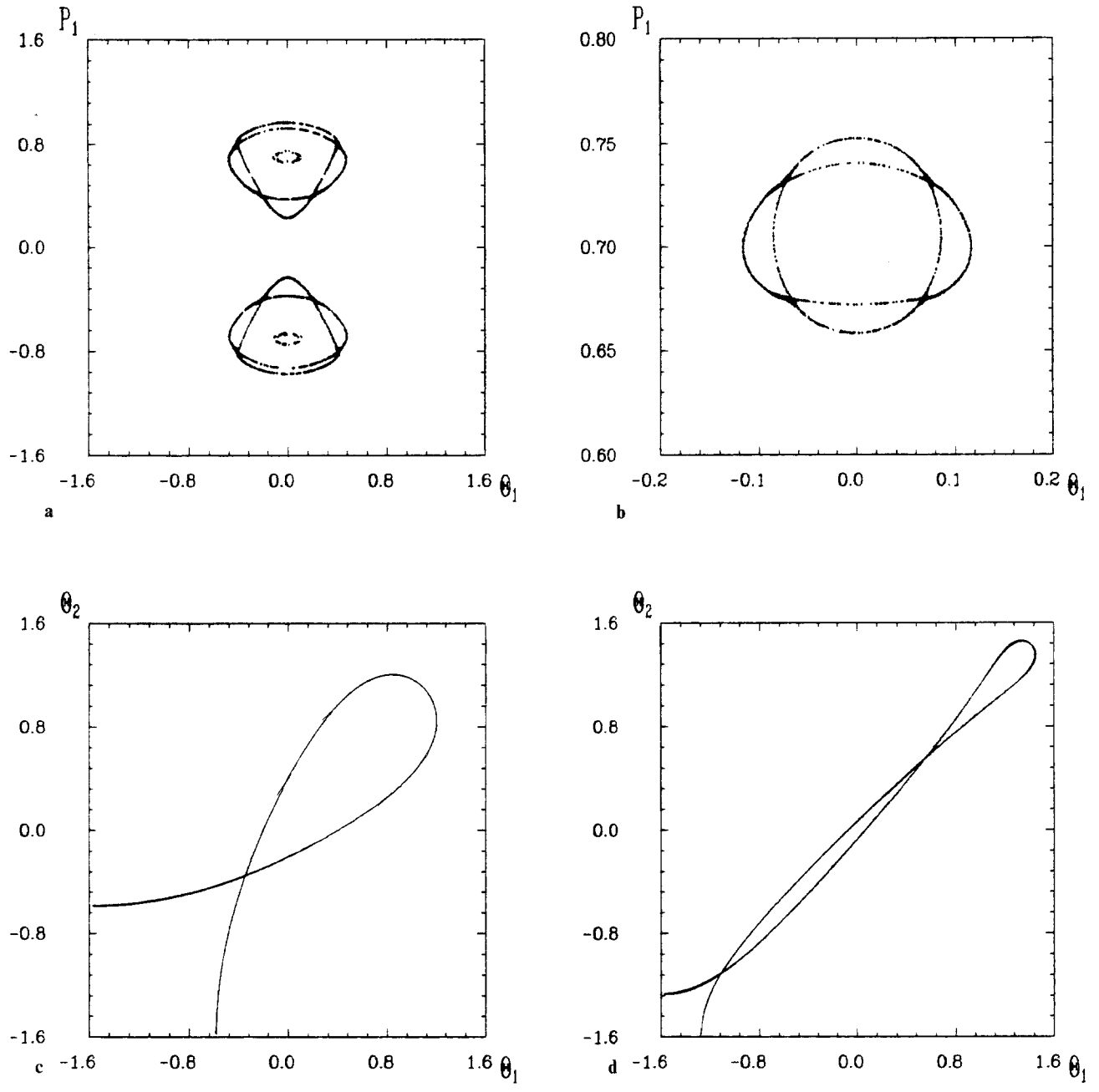

Fig. 7a–d. The self-similarity of the SI for the $(2:n)$-resonances. **a** surface of intersection; **b** enlargement of a; **c** the hyperbolic (2:3) trajectory; **d** the hyperbolic (2:5) trajectory

action integral which are so close to each other that they cannot be evaluated with the usual gaussian approximation. The notion 'close to each other' clearly needs a more precise meaning; however, independent of such a specification, one expects that it depends upon two quantities: the curvature of the action integral at the classical solution, i.e. the eigenvalues of the second variation of the action, and the size of the small parameter, i.e. g_0^2 in our case. The latter defines a 'resolution': the smaller g_0 becomes, the more we are justified to use the usual gaussian approximation, i.e. the more the path integral is able to resolve any given extremum of the action and discern it from the neighbouring ones. The aspect of 'resolution' becomes more transparent if we turn to the ground state wave function: to evaluate it in the semiclassical approximation at a given point in configuration space, we have to sum over all paths which, starting from some toron point, arrive at this point. For a nonintegrable system the semiclassical approximation to the ground state wave function is expected to exhibit strong fluctuations, due to the erratic pattern of classical solutions. Quantum mechanics, on the other hand, is smooth over distances of the mean de Broglie wave length, i.e. on a scale of the order of the small parameter of the Schrödinger equation, which in our case is g_0^2. Therefore, agreement of the semiclassical approximation and the 'true' quantum mechanical solution is obtained only after

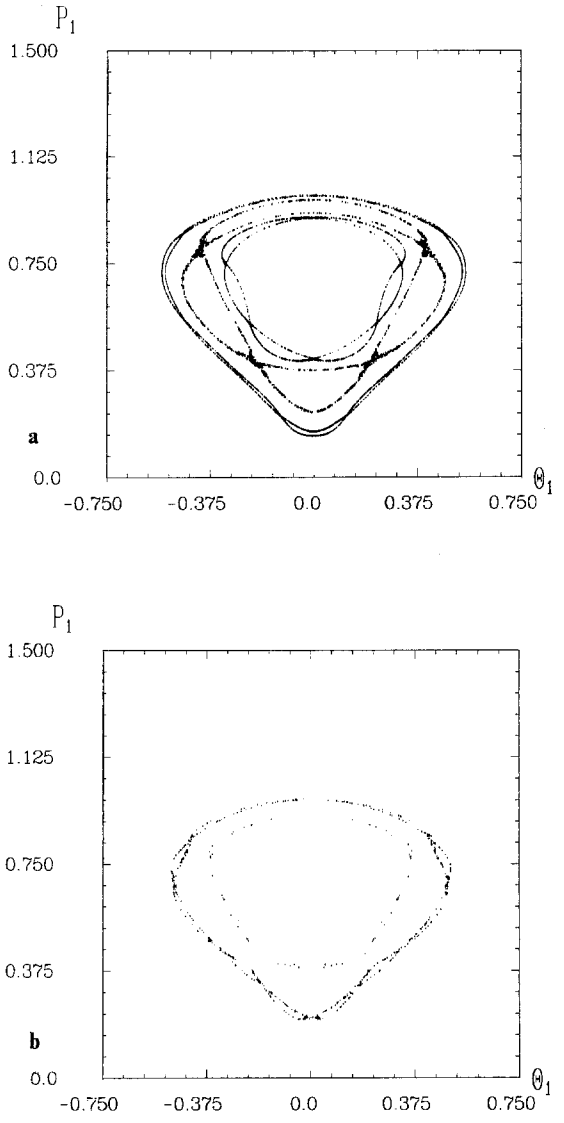

Fig. 8a–b. Accumulation of islands around the (2:3)-resonance. **a** the island chains for the (3:4)-, (2:3)- and (3:5)-resonances (from outside to inside); **b** the (5:7)-resonance (outside) and the (5:8)-resonance (inside)

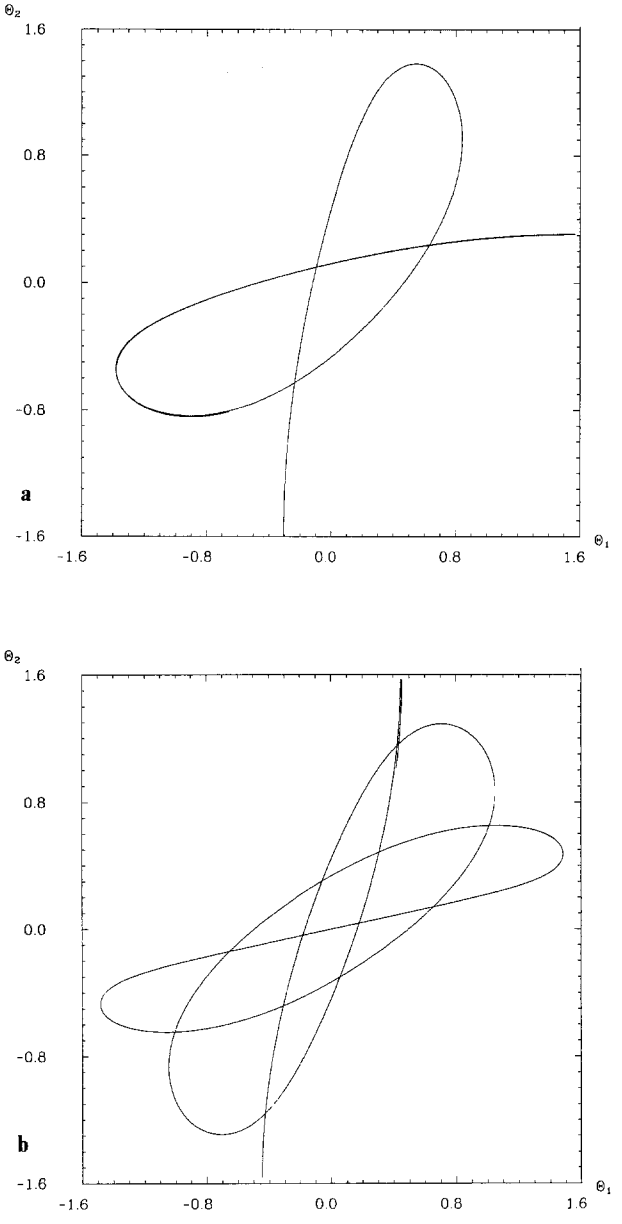

Fig. 9a, b. The trajectory of the (3:4)-resonance; **b** The trajectory of the (5:7)-resonance

averaging the semiclassical wave function over distances of the order g_0^2. On the other hand, the 'true' solution shows more and more of the semiclassical peaking structure, as g_0^2 goes to zero (for a one-dimensional quantum map this has nicely been demonstrated in [22]): in this sense we can say that the resolution increases as g_0^2 becomes smaller and smaller.

Returning to the evaluation of the partition function Z, the actual summation over the classical paths and the calculation of the contribution to Z of the fluctuations around them lies beyond the scope of this paper. Using the results of our numerical computation, we only wish to demonstrate how the number of paths which can be resolved increases as g_0^2 goes to zero. We simply ask, just how many terms one would get in a semiclassical approximation of the path integral, summing all contributions up to some smallest scale, $1/p$ say (the resolution p will go to infinity as g_0^2 goes to zero). For the sake of the argument, let us take the distance of the starting points of the trajectories as a naive measure of their closeness in path space and assume that it is proportional to the difference $m/n_1 - m/n_2$ for the trajectories of an $(m:n_1)$- and an $(m:n_2)$-resonance. To take multiple transversals into account, we denote the trajectory of the $(m:n)$-resonance which is transversed r times by $(rm:rn)$; in the following we shall assume that its action is proportional to rm. Now note that the $(m_1:n_1)$-trajectory transversed r times has an action comparable to that of the $(m_2:n_2)$-trajectory if $m_2 = rm_1$, irrespective of the values of n_1 and n_2. For consistency reasons one should therefore not only sum over all trajectories corresponding to *irreducible* fractions m/n, but also allow for rm/rn, i.e. r

transversals of $(m:n)$-trajectories, as long as their action (assumed to be proportional to rm above) is no larger than that of the trajectory with the largest value of m resolved. Thus the question addressed above reduces to determining the number of rationals m/n, $m<n$, such that

$$\frac{m}{n}-\frac{m}{n+1}>\frac{1}{p}. \tag{5}$$

Asking only for the large p behaviour we may replace sums by integrals and turn the condition (5) on n into $n<\sqrt{mp}$. In this way we obtain

$$\int^{p} \mathrm{d}m \int^{\sqrt{mp}} \mathrm{d}n \sim \int^{p} \mathrm{d}m \sqrt{mp} \propto p^2,$$

i.e. the number of terms is proportional to the square of the resolution and goes to infinity as g_0^2 goes to zero. This large number, together with the expected strong quantum fluctuations, imply that the sum over all these contributions leads to a much larger contribution to the path integral than a single trajectory, as well as some unknown g_0^2-dependence. The crucial question remains whether the number of these trajectories can be large enough and the fluctuations strong enough to compete with the exponential $\exp(-S/g_0^2)$. To answer this question we need more information about the action integrals and their variations near the classical solutions.

We conclude our discussion of the motion in the classically forbidden region with the determination of Lyapunov exponents (see [16, Sect. 5.2.b] or [23]) which we measured for four different trajectories over approximately 10^4 periods. For a trajectory that intersects the SI in the center where appears to be the region of strongest stochasticity (cp. Fig. 3), we found the largest exponent $\sigma_1 \simeq 0.022$. For the trajectories of the (2:3)-resonance (Fig. 7), we obtained a smaller, but still non-zero exponent $\sigma_2 \simeq 0.007$ for the unstable trajectory (Fig. 7c), whereas for the stable trajectory, we got a vanishing exponent $\sigma_3 < 10^{-4}$. Around the diagonal (see Figs. 4–9) we found isolated stable and unstable trajectories that cluster along the diagonal corresponding to elliptic and hyperbolic points in the Poincaré sections. We have been concerned with the study of the latter in the limit $E \to 0$ as these appear as tunneling trajectories in the path integral. For a trajectory in the direct neighbourhood of the diagonal, we measured a non-zero exponent. Its exact evaluation was hampered by the fact that the integration of the motion close to the potential boundary proceeds only very slowly.

3 Discussion

The goal of our analysis was to provide the prerequisites for an evaluation of the path integral in the semiclassical approximation of $SU(2)$ lattice gauge theory, To this end we studied the tunneling trajectories in the space of constant fields described by the Hamiltonian

$$H=\tfrac{1}{2}(p_1^2+p_2^2-\cos^2\theta_1\cos^2\theta_2). \tag{3}$$

For small energies $E \simeq -1/2$ we applied perturbation theory and combined its results with numerical calculations in order to understand the complex behaviour of the system at $E=0$.

Our analysis showed how the tunneling trajectories cluster along the diagonal. We have been looking for solutions which at time $-T$ leave from a toron point and at time $+T$ end at a toron point. Each such trajectory can be labeled by the two integers $(m:n)$, where m indicates how often the trajectory swings along the diagonal before it closes or ends at a toron point and n counts the number of intersections with the diagonal. We then found that the accumulation near the diagonal line can be described by the rational numbers m/n, where m and n are the two labels of the trajectory: the smaller this value, the closer the trajectory lies to the diagonal. In the same way as rational numbers are accumulation points of series of other rationals, each trajectory is an accumulation point for other classical solutions. Furthermore, if we follow, for fixed m, solutions with increasing n, the Poincaré surface of intersection shows a self-repeating structure. Finally, the action integral of these solutions goes approximately as $m \cdot S_0$, where S_0 is the action integral of the diagonal solution.

The task of summing over all these paths has not been attacked in this paper. We have only tried to formulate this problem more precisely. Since many classical paths, i.e. extrema of the action, lie close to each other, the fluctuations around them are expected to be large and the usual gaussian approximation cannot be used. A rough estimate demonstrates that the number of trajectories which, for given g_0, can be resolved grows with p^2 which tends to infinity when g_0 becomes small. This supports the expectation that tunneling along the diagonal line gives a much stronger contribution to the ground state energy split than a single isolated trajectory. Further progress necessitates a better understanding of the nature of the fluctuations around these accumulating trajectories, i.e. the second variation of the action integral.

The self similarity that we have found in the intersection surfaces suggests the use of the renormalization group. Following the arguments of [24], one first defines renormalization group transformations to describe classical solutions on finer and finer scales in phase space. Since in the path integral of quantum mechanical quantities a decrease in g_0 improves the resolution power in phase space and, hence, allows to 'see' classical trajectories on smaller and smaller scales, the same technique should also be useful for the evaluation of path integrals in the semiclassical approximation. As a result one might expect to find some sort of scaling behavior.

References

1. S.G. Matinyan, G.K. Savvidi, N.G. Ter-Arutyunyan-Savvidi: Zh. Eksp. Teor. Fiz. 80 (1981) 830; Sov. Phys. JETP 53 (1981) 421
2. B.V. Chirikov, D.L. Shepelyanskiĭ: Pis'ma Zh. Eksp. Teor. Fiz. 34 (1981) 171; JETP Lett. 34 (1981) 163; E.S. Nikolaevskiĭ, L.N. Shur: Pis'ma Zh. Eksp. Teor. Fiz. 36 (1982) 176; JETP Lett. 36 (1982) 218; E.S. Nikolaevskiĭ, L.N. Shur: Zh. Eksp. Teor. Fiz. 85 (1983) 3; Sov. Phys. JETP 58 (1982) 1; G.K. Savvidy: Phys. Lett. 130B (1983) 303; G.K. Savvidy: Nucl. Phys. B246 (1984) 302
3. B. Simon: Ann. Phys. (N.Y.) 146 (1983) 209; G.K. Savvidy: Phys. Lett. 159B (1985) 325

4. B.V. Medvedev, Teor. Mat. Fiz. 60 (1984) 224; Theor. Math. Phys. 60 (1984) 782; C.C. Martens, R.L. Waterland, W.P. Reinhardt: J. Chem. Phys. 90 (1989) 355
5. A. Carnegie, I.C. Percival: J. Phys. A17 (1984) 801; S.-J. Chang: Phys. Rev. D29 (1984) 259; W.-H. Steeb, C.M. Villet, A. Kunick: J. Phys. A18 (1985) 3269; G. Sohos, T. Bountis, H. Polymilis, Nuovo Cimento B104 (1989) 339; P. Dahlqvist, G. Russberg: Phys. Rev. Lett. 65 (1990) 2837
6. M. Lüscher: Nucl. Phys. B219 (1983) 233
7. M. Lüscher, G. Münster: Nucl. Phys. B232 (1984) 445
8. P. van Baal, J. Koller: Ann. Phys. (N.Y.) 174 (1987) 299
9. J. Koller, P. van Baal: Nucl. Phys. B302 (1988) 1
10. P. van Baal: Phys. Lett. 224B (1989) 397; P. van Baal: Nucl. Phys. B (Proc. Suppl.) 17 (1990) 581
11. B. Berg, A. Billoire: Phys. Rev. D40 (1989) 550; C. Michael, G.A. Tickle, M.J. Teper: Phys. Lett. 207B (1988) 313; P. van Baal, A. Kronfeld; Nucl. Phys. B (Proc. Suppl.) 9 (1989) 227
12. J. Bartels, T.T. Wu: Phys. Rev. D37 (1988) 2307
13. J. Bartels, B. Raabe, T.T. Wu: Phys. Rev. D42 (1990) 1233
14. A.M. Polyakov: Nucl. Phys. B120 (1977) 429
15. S. Coleman: The uses of instantons. in: A. Zichichi (ed.), The whys of subnuclear physics, Proceedings Erice 1977, p. 805 New York: Plenum 1979
16. A.J. Lichtenberg, M.A. Lieberman: Regular and stochastic motion, Berlin, Heidelberg, New York: Springer 1983
17. G.H. Walker, J. Ford: Phys. Rev. 188 (1969) 416
18. M. Hénon, C. Heiles: Astron. J. 69 (1964) 73
19. M. Abramowitz, I.A. Stegun (eds.): Handbook of mathematical functions, 9th edition. New York: Dover 1970
20. L.D. Landau, E.M. Lifschitz: Mechanik, 11th edition, Chap. 10. Berlin: Akademie Verlag 1984
21. M. Berry: Semiclassical mechanics of regular and irregular motion, in: G. Iooss, R.H.G. Helleman, R. Stora (eds.), Chaotic behaviour of deterministic systems, Proceedings Les Houches 1981, p. 171 Amsterdam: North Holland 1983
22. M.V. Berry, N.L. Balazs, M. Tabor, A. Voros: Ann. Phys. (N.Y.) 122 (1979) 26
23. J.M. Greene, J.-S. Kim: Physica D24 (1987) 213
24. D.F. Escande: Phys. Rep. 121 (1985) 165